scientific reports

Check for updates

OPEN

Optimization of machine tool settings for Spirac hypoid gears by controlling symmetry of contact paths

Jiamin Xuan[1]✉, Haitao Li[2] & Wei Zhang[1]

A novel optimization method to control the symmetry of contact paths on the concave and convex tooth surfaces of the gear then improves the meshing quality was proposed. By modifying the angular setting of the head cutter when cutting the pinion, the direction angles of the two contact paths are equated to estimate their symmetry. The relation between the direction angles is formulated precisely, the influence of the angular setting on the contact paths is investigated, and the equations for obtaining the values of the machine tool settings are derived. The proposed method is applied to a numerical example of a Spirac hypoid gear pair, and the results reveal that the contact paths on the concave and convex tooth surfaces are approximately symmetrical and the transmission errors of both sides are comparable.

Keywords Hypoid gears, Direction angle of contact path, Spirac hypoid gears, Machine tool setting, Face-hobbing

Hypoid gears are widely used to transfer power between two non-intersecting crossed axes, mostly found in the front and the rear axles of all-wheel-drive vehicles or in the rear axles of rear-wheel-drive ones[1,3]. Furthermore, most hypoid gears are manufactured by either the face-milling method or the face-hobbing method[2–4]. The face-milling method mainly depends on local syntheses[5–8], which predetermine the contact characteristics of the pinion and the gear at a mean point, including the direction of the contact path. Besides determining the contact characteristics around the mean point, Wu et al.[9] presented a theory for the function-oriented design of point contact tooth surfaces. The theory was applied to determine the contact path, major axial length of the instantaneous contact ellipse, and higher-order acceleration as required. Compared with the face-milling method, the face-hobbing method only considers the first-order parameters at the mean point in computing the machine tool settings, such as the position of the reference point, pressure angle, and spiral angle at the reference point; nevertheless, it does not consider the contact path[10]. To guarantee the quality of hypoid gears, various strategies, including higher-order modifications to correct the tooth flank form machining errors[11,12], ease-off flank modifications for tooth correction and meshing performance improvement[13–15], and multi-objective tooth optimization with modification-based loaded tooth contact analysis to improve the overall meshing quality[16,17] have been proposed. However, most of them are based on Gleason's hypoid generator.

There are three common face-hobbing systems for computing the machine tool settings for hypoid gears, including Klingelnberg's CycloPalloid system, Oerlikon's Spirac and Spiroflex systems, and Gleason's Phoenix system[4,18]. In the Spiroflex system, the pinion and the gear are cut using the generated method; the contact paths on the concave and convex tooth surfaces of the gear are approximately symmetrical, and the instantaneous contact ellipses at the reference point are also symmetrical. However, in the Spirac system, the pinion is cut by the generated method, the gear is cut by the nongenerated method (which enhances production), and the symmetry of the contact paths cannot be guaranteed. Consequently, the contact paths must be modified artificially and repeatedly by correcting the machine tool settings during the tooth contact analysis. The Spirac system is applicable under two conditions for the hypoid gears: when the transmission ratio is greater than or equal to 3 and when the pitch angle of the gear is greater than or equal to 60°[10]. Generally, the hypoid gears cut by the Spirac system are called Spirac hypoid gears. For Spirac hypoid gears, few studies have been conducted to develop a universal hypoid generator mathematical model[19], a flank-correction methodology from the six-axis

[1]Cryogenic fluid equipment R&D Zhejiang Engineering Research Center, Zhejiang Institute of Mechanical and Electrical Engineering, Hangzhou 310053, Zhejiang, China. [2]College of Engineering, China Agricultural University, Beijing 100083, China. ✉email: xuanjiamin@zime.edu.cn

Cartesian-type CNC hypoid generator[18], anew analytical method for the basic machine tool settings to realize conjugated action[20], an active tooth surface–design methodology based on coordinate measurements[21], etc.

The contact path is one of the dominant factors governing the load behaviors of hypoid gears [10]. In this paper, a new method is proposed to calculate the machine tool settings for Spirac hypoid gears. It controls the direction angles of the contact paths to be equated to achieve symmetrical contact paths on both tooth surfaces of the gear. Furthermore, the relation between the direction angles is formulated, the influence of the angular setting of the pinion head cutter on the contact paths is determined, and the equations to solve for the values of the machine tool settings are derived. The computation is tested using a numerical example.

Theoretical background

In the face-hobbing method, the cutting of tooth surfaces is a continuous indexing process. As shown in Fig. 1, the concave and convex tooth surfaces of a tooth slot are manufactured simultaneously using blade groups[12]. Each blade group contains an inside blade and an outside one, which are placed at the same reference circle on the pitch plane of the head cutter. In the face-hobbing method, the traces of the cutting edges of the head cutter blades form the teeth of virtual generating gear. The curve of the tooth trace of the generating gear forms an extended epicycloid.

In the generated method, two sets of related motions are defined: the relative rotation between the head cutter and the blank, and the rolling (or generating) motion, corresponding to the relative rotation between the virtual generating gear and the blank. In the nongenerated method, which is usually applied to the gear, only the indexing motion is considered.

Generation of the gear tooth surface

When the gear is cut by the nongenerated method, the trace of the blade on the blank is the tooth surface of the gear. Figure 2 shows the relative position between the head cutter and the gear with the right-hand teeth. The reference plane, T, is the basis of the relative position between the gear and the generating gear. P_0 is the pitch point of the blades and its distance to the axis of the head cutter is the nominal cutter radius (r_0). T_0 is a plane parallel to plane T and that passes through point P_0 with the addendum modification (h_{x2}). T' is a plane perpendicular to the axis of the head cutter and rotating about point P_0 by tilt angle of the head cutter (χ_2). M is the reference point of either the pinion or the gear. In order to accommodate the correct orientation with respect to the cutting motion vector, the effective cutting direction of the blades in the head cutter is not perpendicular to the cutter radius vector. δ_{02} is the angle between the cutting direction of the blade and the cutter radius vector. β_{m2} is the mean spiral angle of the gear at point M. R_{m2} is the gear cone distance of point M. r_{m2} is the radius of the reference circle at point M. δ_{M2} is the gear installment angle. When angle δ_{M2} equals the gear pitch angle δ_2, origin O_p coincides with the gear pitch cone apex O'_2.

Coordinate system $S(O; \boldsymbol{i}, \boldsymbol{j}, \boldsymbol{k})$ is rigidly connected to the head cutter, where origin O is at the intersection point of plane T' and the axis of the head cutter, axis $\boldsymbol{i}$ directs to point P_0, and axis $\boldsymbol{k}$ coincides with the axis of the head cutter. Coordinate system $S_0(O'_0; \boldsymbol{i}_0, \boldsymbol{j}_0, \boldsymbol{k}_0)$ is an auxiliary coordinate system, where origin O'_0 is at the intersection point of plane T_0 and the axis of the head cutter, axis $\boldsymbol{i}_0$ directs to point P_0, and axis $\boldsymbol{k}_0$ is perpendicular to plane T_0. Origin O_0 is at the intersection point of plane T and axis $\boldsymbol{k}_0$, initially located based on the radial setting (E_{x2}) and the angular setting (q_2) in coordinate system $S_p(O_p; \boldsymbol{i}_p, \boldsymbol{j}_p, \boldsymbol{k}_p)$. Axis $\boldsymbol{i}_p$ passes through point M, and axis $\boldsymbol{k}_p$ coincides with axis $\boldsymbol{k}_0$. Coordinate system $S_2(O''_2; \boldsymbol{i}_2, \boldsymbol{j}_2, \boldsymbol{k}_2)$ is rigidly connected to the gear, where origin O''_2 is at the center of the reference circle of the gear; axis $\boldsymbol{i}_2$ passes through point M, axis $\boldsymbol{j}_2$ coincides with axis $\boldsymbol{j}_p$, and axis $\boldsymbol{k}_2$ coincides with the axis of the gear and points to the heel.

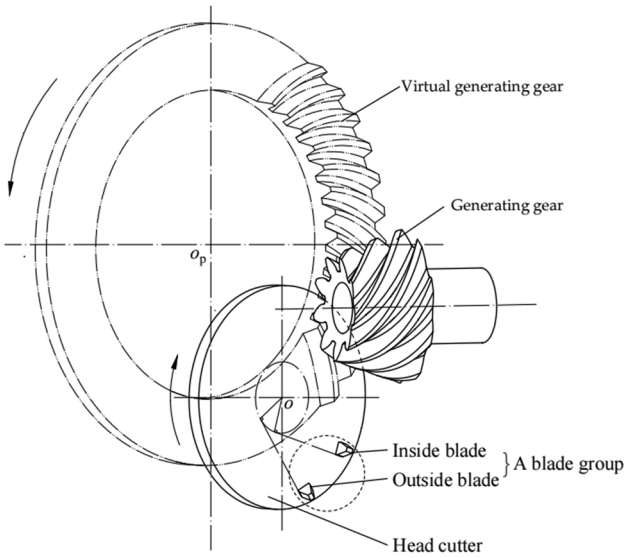

Figure 1. Face-hobbing method.

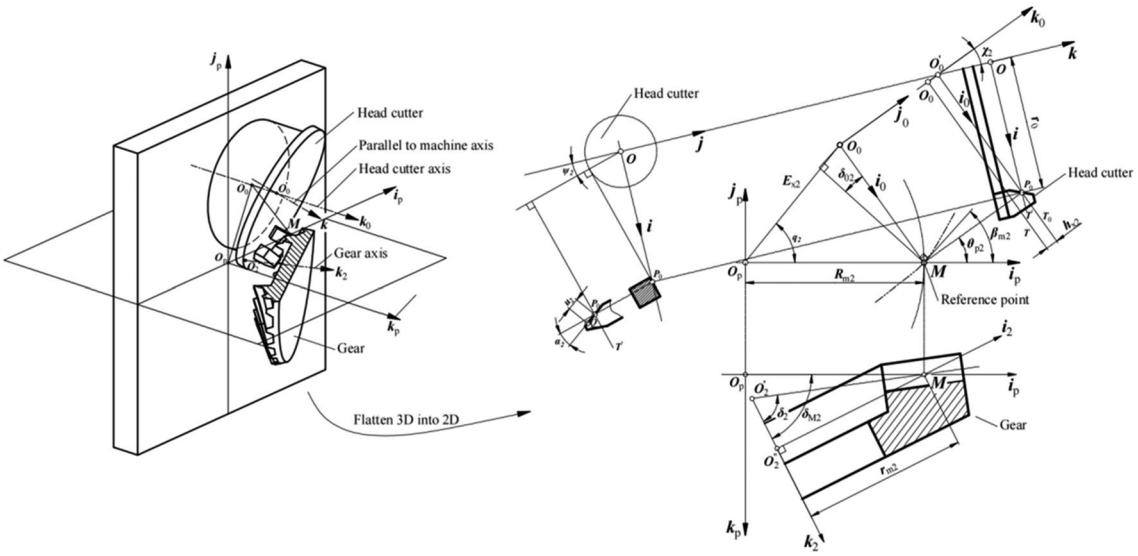

Figure 2. Relative position between the head cutter and the gear with the right-hand teeth.

The trace of the cutting edge of the head cutter blade is presented in coordinate system S (rigidly connected to the head cutter) by the vector-parametric equation (fully described in Reference[22]):

$$(\boldsymbol{R}_2) = \boldsymbol{OP}_0 + \boldsymbol{P}_0\boldsymbol{Q} = \boldsymbol{R}_2(u_2, \psi_2, \alpha_2), \tag{1}$$

Where $(\boldsymbol{R}_2)$ is a position vector of an arbitrary point of the trace of the cutting edge; u_2 is the distance from the intersection point of the edge of the blade and plane T' to an arbitrary point along the edge of the blade; ψ_2 is the angle of rotation of the head cutter; α_2 is the blade angle. The subscript inside the parentheses indicates the number of a body the considered quantity belongs to (index 1 indicates a pinion, index 2 indicates a gear, index 4 indicates a generating gear of pinion). The subscript outside the parentheses indicates a coordinate system in which the considered vector is defined.

The gear tooth surface (Σ_2) produced by coordinate transformation from coordinate system S to coordinate system S_2 (connected to the gear) is defined by the following equation (based on Fig. 2)[22]:

$$(\boldsymbol{r}_2^*)_2 = \boldsymbol{M}_{22} \cdot \boldsymbol{M}_{P2} \cdot \boldsymbol{M}_{20P} \cdot \boldsymbol{M}_{20} \cdot (\boldsymbol{R}_2), \tag{2}$$

The coordinate transformations between coordinate systems S, S_0, S_p, S_2 (Fig. 2), are performed as it follows:

$$(\boldsymbol{R}_2)_0 = \boldsymbol{M}_{20} \cdot (\boldsymbol{R}_2) = \begin{bmatrix} cos\chi_2 & 0 & sin\chi_2 & 0 \\ 0 & 1 & 0 & 0 \\ -sin\chi_2 & 0 & cos\chi_2 & r_0 \cdot tan\chi_2 \\ 0 & 0 & 0 & 1 \end{bmatrix} \cdot (\boldsymbol{R}_2), \tag{3}$$

$$(\boldsymbol{r}_2)_p = \boldsymbol{M}_{20P} \cdot (\boldsymbol{R}_2)_0 = \begin{bmatrix} cos(\theta_{p2} - 90^\circ) & -sin(\theta_{p2} - 90^\circ) & 0 & E_{x2} \cdot cosq_2 \\ sin(\theta_{p2} - 90^\circ) & cos(\theta_{p2} - 90^\circ) & 0 & E_{x2} \cdot sinq_2 \\ 0 & 0 & 1 & h_{x2} \\ 0 & 0 & 0 & 1 \end{bmatrix} \cdot (\boldsymbol{R}_2)_0, \tag{4}$$

$$(\boldsymbol{r}_2)_2 = \boldsymbol{M}_{P2} \cdot (\boldsymbol{r}_2)_p = \begin{bmatrix} sin\delta_{M2} & 0 & -cos\delta_{M2} & R_{m2} - r_{m2} \cdot sin\delta_{M2} \\ 0 & 1 & 0 & 0 \\ cos\delta_{M2} & 0 & sin\delta_{M2} & r_{m2} \cdot cos\delta_{M2} \\ 0 & 0 & 0 & 1 \end{bmatrix} \cdot (\boldsymbol{r}_2)_p, \tag{5}$$

Where

$$\theta_{p2} = \beta_{m2} - \delta_{02}. \tag{6}$$

To obtain surface Σ_2 in the generating process, the head cutter is rolled with the work gear, and surface Σ_2 are defined by the following:

$$(\boldsymbol{r}_2^*)_2 = \boldsymbol{M}_{22} \cdot (\boldsymbol{r}_2)_2 = \begin{bmatrix} cos(i_{20} \cdot \psi_2) & -sin(i_{20} \cdot \psi_2) & 0 & 0 \\ sin(i_{20} \cdot \psi_2) & cos(i_{20} \cdot \psi_2) & 0 & 0 \\ 0 & 0 & 1 & 0 \\ 0 & 0 & 0 & 1 \end{bmatrix} \cdot (\boldsymbol{r}_2)_2 = [x_2 y_2 z_2 1]^T, \tag{7}$$

Where the velocity ratio i_{20} in the kinematic scheme of the head cutter for the generation of gear tooth surfaces, based on the ratio of the numbers of blades (z_0) and teeth (z_2), is:

$$i_{20} = \frac{z_0}{z_2}. \tag{8}$$

The unit normal vector to surface Σ_2 at point M in coordinate system S_2 is:

$$(\boldsymbol{n}_2^*)_2 = \frac{\left(\boldsymbol{r}_{2u}^*\right)_2 \times \left(\boldsymbol{r}_{2\psi}^*\right)_2}{\left|\left(\boldsymbol{r}_{2u}^*\right)_2 \times \left(\boldsymbol{r}_{2\psi}^*\right)_2\right|} = \frac{\frac{\partial (\boldsymbol{r}_2^*)_2}{\partial u_2} \times \frac{\partial (\boldsymbol{r}_2^*)_2}{\partial \psi_2}}{\left|\frac{\partial (\boldsymbol{r}_2^*)_2}{\partial u_2} \times \frac{\partial (\boldsymbol{r}_2^*)_2}{\partial \psi_2}\right|} \tag{9}$$

Generation of the generating gear tooth surface of pinion

In the generated method, the generation of the pinion is based on the concept of the virtual generating gear, and the pinion tooth surface (Σ_1) is generated as an envelope of the virtual generating gear (Σ_4). Figure 3 shows the relative position between the head cutter, generating gear of pinion, and pinion with the left-hand teeth. The virtual generating gear is similar to the gear. h_{x1} is the addendum modification, and χ_1 is the tilt angle of the head cutter. Coordinate systems S and S_0 are established similar to the coordinate systems of the gear shown in Fig. 2. Coordinate system $S_4(O_4; \boldsymbol{i}_4, \boldsymbol{j}_4, \boldsymbol{k}_4)$ is connected to the virtual generating gear, where origin O_4 is at the center of the pitch circle of the generating gear, axis $\boldsymbol{i}_4$ passes through point M, axis $\boldsymbol{j}_4$ coincides with axis $\boldsymbol{j}_p$, and axis $\boldsymbol{k}_4$ coincides with the axis of the generating gear of pinion. Origin O_0 is at the intersection point of plane T and axis $\boldsymbol{k}_0$, initially located based on the radial setting (E_{x1}) and the angular setting (q_1) in coordinate system $S_p(O_p; \boldsymbol{i}_p, \boldsymbol{j}_p, \boldsymbol{k}_p)$. δ_4 is the pitch angle of the generating gear. δ_{40} is the generating gear installment angle.

The movable coordinate system S_4 is rigidly connected with the generating gear of pinion. It is constructed by analogy to system S_4. The generating gear tooth surface of pinion (Σ_4) and the unit normal to surface Σ_4 at point M are [22]

$$(\boldsymbol{r}_4^*)_4 = \boldsymbol{M}_{44} \cdot \boldsymbol{M}_{P4} \cdot \boldsymbol{M}_{40P} \cdot \boldsymbol{M}_{40} \cdot (\boldsymbol{R}_4) = [x_4 y_4 z_4 1]^T, \tag{10}$$

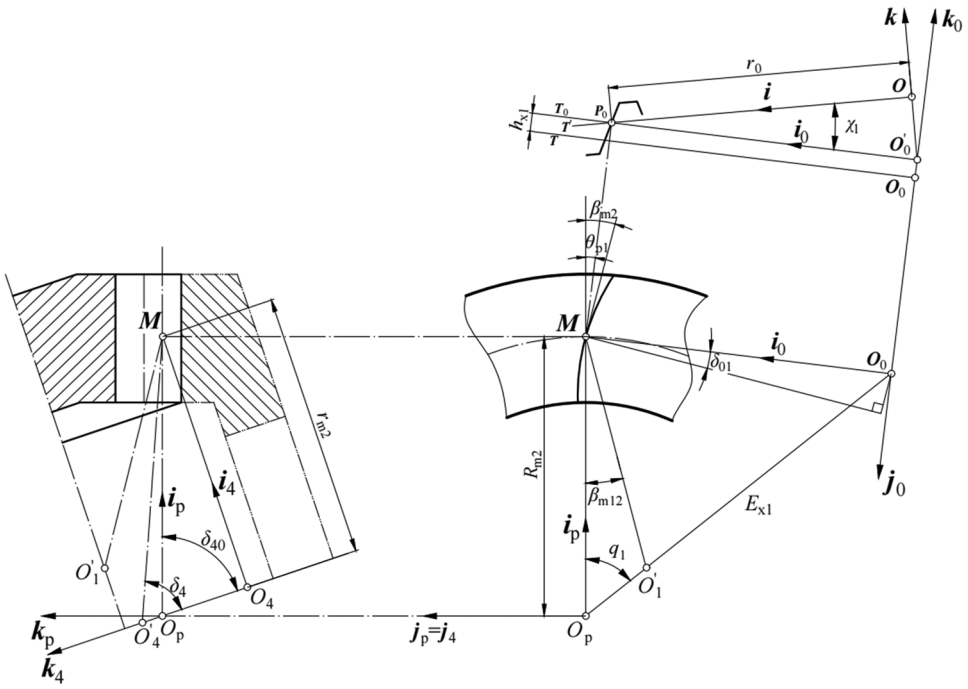

Figure 3. Positions of the head cutter, generating gear, and pinion with the left-hand teeth.

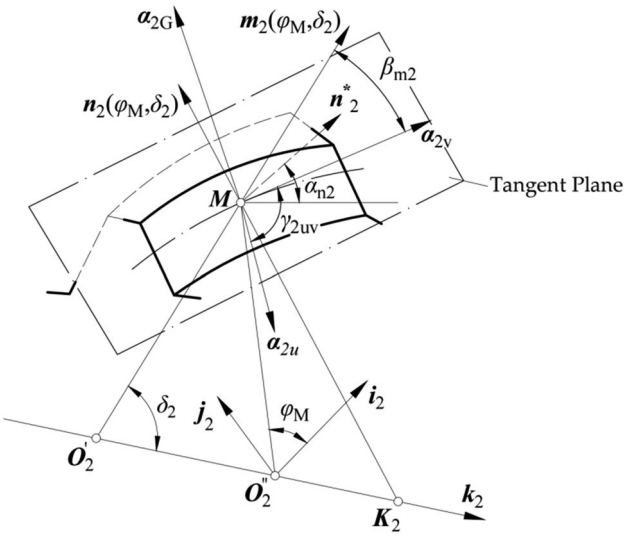

Figure 4. Positions of the tangent vectors to the parameter curves, tooth profile curve, and toothtrace curve at point *M*.

$$(n_4^*)_4 = \frac{\left(r_{4u}^*\right)_4 \times \left(r_{4\psi}^*\right)_4}{\left|\left(r_{4u}^*\right)_4 \times \left(r_{4\psi}^*\right)_4\right|} = \frac{\frac{\partial (r_4^*)_4}{\partial u_1} \times \frac{\partial (r_4^*)_4}{\partial \psi_1}}{\left|\frac{\partial (r_4^*)_4}{\partial u_1} \times \frac{\partial (r_4^*)_4}{\partial \psi_1}\right|}. \tag{11}$$

Here, (R_4) is a position vector of an arbitrary point of the trace of the cutting edge, presented in system S by the vector-parametric equation (fully described in Reference 22):

$$(R_4) = R_4(u_1, \psi_1, \alpha_1), \tag{12}$$

Where u_1 is the distance from the intersection point of the edge of the blade and plane T' to an arbitrary point along the edge of the blade, ψ_1 is the angle of rotation of the head cutter, and α_1 is the blade angle. Subscript 4 inside the parentheses indicates the parameter of the generating gear of the pinion. x_4, y_4, and z_4 are Cartesian coordinates representing the position of $(r^*{}_4)_4$.

Matrices M_i provide the coordinate transformations from coordinate systems S to S_4, defined by equations:

$$(R_4)_0 = M_{40} \cdot (R_4) = \begin{bmatrix} cos\chi_1 & 0 & sin\chi_1 & 0 \\ 0 & 1 & 0 & 0 \\ -sin\chi_1 & 0 & cos\chi_1 & r_0 \cdot tan\chi_1 \\ 0 & 0 & 0 & 1 \end{bmatrix} \cdot (R_4), \tag{13}$$

$$(r_4)_p = M_{40P} \cdot (R_4)_0 = \begin{bmatrix} cos\left(\theta_{p1} - 90^\circ\right) & -sin\left(\theta_{p1} - 90^\circ\right) & 0 & E_{x1} \cdot cosq_1 \\ sin\left(\theta_{p1} - 90^\circ\right) & cos\left(\theta_{p1} - 90^\circ\right) & 0 & E_{x1} \cdot sinq_1 \\ 0 & 0 & 1 & h_{x1} \\ 0 & 0 & 0 & 1 \end{bmatrix} \cdot (R_4)_0, \tag{14}$$

$$(r_4)_4 = M_{P4} \cdot (r_4)_p = \begin{bmatrix} sin\delta_{40} & 0 & cos\delta_{40} & R_{m2} - r_{m2} \cdot sin\delta_{40} \\ 0 & 1 & 0 & 0 \\ -cos\delta_{40} & 0 & sin\delta_{40} & -r_{m2} \cdot cos\delta_{40} \\ 0 & 0 & 0 & 1 \end{bmatrix} \cdot (r_4)_p, \tag{15}$$

Where

$$\theta_{p1} = \beta_{m1} - \delta_{01}, \tag{16}$$

Matrix M_{44} defines the relation between the pinion and its generating gear rotating through mesh, and it is described by the following equation (Fig. 3):

$$(r_4^*)_4 = M_{44} \cdot (r_4)_4 = \begin{bmatrix} cos(i_{20} \cdot \psi_1) & -sin(i_{20} \cdot \psi_1) & 0 & 0 \\ sin(i_{20} \cdot \psi_1) & cos(i_{20} \cdot \psi_1) & 0 & 0 \\ 0 & 0 & 1 & 0 \\ 0 & 0 & 0 & 1 \end{bmatrix} \cdot (r_4)_4. \tag{17}$$

Curvature parameters of the tooth surfaces in the tooth trace and tooth profile directions at the reference point

Each of the tooth surfaces described above covers two families of parameter curves, namely, the u-parameter curve and the ψ-parameter curve. For each point on surface Σ_2, tangent vector $\boldsymbol{\alpha}_{2u}$ to the u-parameter curve and tangent vector $\boldsymbol{\alpha}_{2\psi}$ to the ψ-parameter curve are represented in coordinate system S_2, as follows (based on Fig. 4):

$$(\boldsymbol{\alpha}_{2u})_2 = \frac{\left(\boldsymbol{r}^*_{2u}\right)_2}{\left|\left(\boldsymbol{r}^*_{2u}\right)_2\right|}, \tag{18}$$

$$\left(\boldsymbol{\alpha}_{2\psi}\right)_2 = \frac{\left(\boldsymbol{r}^*_{2\psi}\right)_2}{\left|\left(\boldsymbol{r}^*_{2\psi}\right)_2\right|}. \tag{19}$$

The angle between vector $\boldsymbol{\alpha}_{2u}$ and vector $\boldsymbol{\alpha}_{2\psi}$ is determined by

$$\gamma_{2u\psi} = arccos\left[(\boldsymbol{\alpha}_{2u})_2 \cdot (\boldsymbol{\alpha}_{2\psi})_2\right]. \tag{20}$$

The normal curvature and the geodesic torsion of surface Σ_2 for the directions of the u-parameter curve and the ψ-parameter curve are determined and denoted by κ_{2u}, τ_{2u}, $\kappa_{2\psi}$ and $\tau_{2\psi}$, respectively:

$$\kappa_{2u} = 0, \tag{21}$$

$$\kappa_{2\psi} = \frac{(\boldsymbol{n}^*_2)_2 \cdot \left(\boldsymbol{r}^*_{2\psi\psi}\right)_2}{\left[\left(\boldsymbol{r}^*_{2\psi}\right)_2\right]^2} = \frac{(\boldsymbol{n}^*_2)_2 \cdot \frac{\partial^2 (\boldsymbol{r}^*_2)_2}{(\partial \psi_2)^2}}{\left[\frac{\partial (\boldsymbol{r}^*_2)_2}{\partial \psi_2}\right]^2}, \tag{22}$$

$$\tau_{2u} = \frac{(\boldsymbol{n}^*_2)_2 \cdot \left(\boldsymbol{r}^*_{2u\psi}\right)_2}{\sqrt{\left[\left(\boldsymbol{r}^*_{2u}\right)_2\right]^2\left[\left(\boldsymbol{r}^*_{2\psi}\right)_2\right]^2 - \left[\left(\boldsymbol{r}^*_{2u}\right)_2 \cdot \left(\boldsymbol{r}^*_{2\psi}\right)_2\right]^2}} = \frac{(\boldsymbol{n}^*_2)_2 \cdot \frac{\partial^2 (\boldsymbol{r}^*_2)_2}{\partial \psi_2 \partial u_2}}{\sqrt{\left[\frac{\partial (\boldsymbol{r}^*_2)_2}{\partial u_2}\right]^2\left[\frac{\partial (\boldsymbol{r}^*_2)_2}{\partial \psi_2}\right]^2 - \left[\left(\frac{\partial (\boldsymbol{r}^*_2)_2}{\partial u_2}\right)_2 \cdot \frac{\partial (\boldsymbol{r}^*_2)_2}{\partial \psi_2}\right]^2}}, \tag{23}$$

$$\tau_{2\psi} = \frac{\kappa_{2\psi} \cdot \left(\boldsymbol{r}^*_{2u}\right)_2 \cdot \left(\boldsymbol{r}^*_{2\psi}\right)_2}{\sqrt{\left[\left(\boldsymbol{r}^*_{2u}\right)_2\right]^2\left[\left(\boldsymbol{r}^*_{2\psi}\right)_2\right]^2 - \left[\left(\boldsymbol{r}^*_{2u}\right)_2 \cdot \left(\boldsymbol{r}^*_{2\psi}\right)_2\right]^2}} - \tau_{2u} \tag{24}$$

As shown in Figs. 4 and 5, an initial position of the gear is the position in which the reference point M, located in the gear pitch cone generatrix. Angle φ_M of the gear rotation about its axis $\boldsymbol{k}_2$ is measured from initial positions. Vector $\boldsymbol{m}_2(\varphi_M, \delta_2)$ is the unit vector of the gear pitch cone generatrix and $\boldsymbol{n}_2(\varphi_M, \delta_2)$ is the normal vector of the gear pitch cone surface at point M (Fig. 4). Parameter α_{n2} is the pressure angle of the gear tooth surface at point M. $\boldsymbol{\alpha}_{2v}$ is the unit vector for the direction of the tooth trace, and $\boldsymbol{\alpha}_{2G}$ is the unit vector for the direction of the tooth profile. $\boldsymbol{\alpha}_{2v}$ is perpendicular to $\boldsymbol{\alpha}_{2G}$. $\boldsymbol{\alpha}_{2v}$ and $\boldsymbol{\alpha}_{2G}$ are in the tangent planes to surface Σ_2 at point M, and $\boldsymbol{\alpha}_{2v}$ can be represented in coordinate system S_2 as:

$$(\boldsymbol{\alpha}_{2v})_2 = \frac{\boldsymbol{n}_2(\varphi_{M2}, \delta_2) \times (\boldsymbol{n}^*_2)_2}{sin(90^\circ - \alpha_n)}, \tag{25}$$

$$(\boldsymbol{\alpha}_{2G})_2 = (\boldsymbol{\alpha}_{2v})_2 \times (\boldsymbol{n}^*_2)_2. \tag{26}$$

Here,

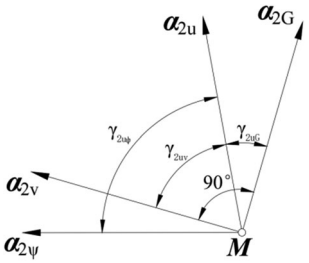

Figure 5. Directions of the tangent vectors to the parameter curves, tooth profile curve, and tooth trace curve at M.

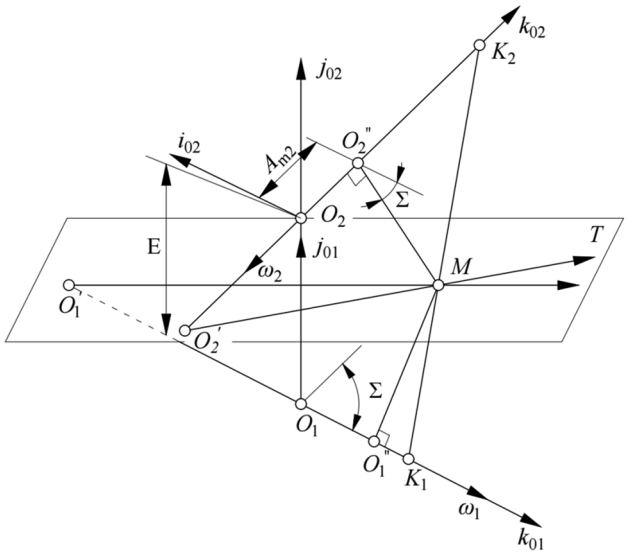

Figure 6. Coordinate systems connected to the machine frame.

$$\boldsymbol{n}_2(\varphi_{M2}, \delta_2) = \begin{bmatrix} cos\delta_2 cos\varphi_{M2} \\ cos\delta_2 sin\varphi_{M2} \\ -sin\delta_2 \\ 1 \end{bmatrix}, \tag{27}$$

$$\varphi_{\mathrm{M2}} = arctan(\frac{y_2}{x_2}), \tag{28}$$

$$\alpha_n = arcsin\left[\boldsymbol{n}_2(\varphi_{M2}, \delta_2) \cdot (\boldsymbol{n}_2^*)_2\right]. \tag{29}$$

The angle between vectors $\boldsymbol{\alpha}_{2\mathrm{u}}$ and $\boldsymbol{\alpha}_{2\mathrm{v}}$ is determined by

$$\gamma_{2u\psi} = arccos[(\boldsymbol{\alpha}_{2\mathrm{u}})_2 \cdot (\boldsymbol{\alpha}_{2\mathrm{v}})_2]. \tag{30}$$

The normal curvatures and the geodesic torsion for the directions of the tooth trace and the tooth profile can be represented respectively by.

$$\kappa_{2\mathrm{v}} = \left[\kappa_{2\psi} + (\tau_{2\psi} - \tau_{2\mathrm{u}})/tan\gamma_{2\mathrm{u}\psi}\right] sin^2\gamma_{2\mathrm{uv}} + \tau_{2\mathrm{u}} sin2\gamma_{2\mathrm{uv}}. \tag{31}$$

$$\kappa_{2\mathrm{G}} = \left[\kappa_{2\psi} + (\tau_{2\psi} - \tau_{2\mathrm{u}})/tan\gamma_{2\mathrm{u}\psi}\right] cos^2\gamma_{2\mathrm{uv}} - \tau_{2\mathrm{u}} sin2\gamma_{2\mathrm{uv}}. \tag{32}$$

$$\tau_{2\mathrm{v}} = 0.5\left[\kappa_{2\psi} + (\tau_{2\psi} - \tau_{2\mathrm{u}})/tan\gamma_{2\mathrm{u}\psi}\right] sin2\gamma_{2\mathrm{uv}} + \tau_{2\mathrm{u}} cos2\gamma_{2\mathrm{uv}}. \tag{33}$$

$$\tau_{2\mathrm{G}} = -\tau_{2\mathrm{v}} \tag{34}$$

The normal curvatures and the geodesic torsion of the generating gear tooth surface Σ_4 of the pinion for the directions of the tooth trace and the tooth profile can be represented and denoted respectively by $\kappa_{4\mathrm{v}}$, $\tau_{4\mathrm{v}}$, $\kappa_{4\mathrm{G}}$, $\tau_{4\mathrm{G}}$, and $\gamma_{4\mathrm{uv}}$, $\gamma_{4\mathrm{u}\psi}$. The detailed derivations, fully provided in Reference 22, are the same as Eqs. (18–34).

In the generation method, the pinion tooth surface Σ_1 is the envelope of the family of generating surfaces Σ_4. Based on the meshing theory, the normal curvatures and the geodesic torsion ($\kappa_{1\mathrm{v}}$, $\kappa_{1\mathrm{G}}$, and $\tau_{1\mathrm{v}}$) of surface Σ_1 for tangent vectors $\boldsymbol{\alpha}_{1\mathrm{v}}$ and $\boldsymbol{\alpha}_{1\mathrm{G}}$ of the tooth trace and the tooth profile at point M are determined with respect to the curvature relations between the mating surfaces and represented by the following equations:

$$\kappa_{1\mathrm{v}} = \kappa_{4\mathrm{v}} - \kappa_{41\mathrm{v}}. \tag{35}$$

$$\kappa_{1\mathrm{G}} = \kappa_{4\mathrm{G}} - \kappa_{41\mathrm{G}}. \tag{36}$$

$$\tau_{1\mathrm{v}} = \tau_{4\mathrm{v}} - \tau_{41\mathrm{v}}. \tag{37}$$

Here, $\kappa_{41\mathrm{v}}$, $\kappa_{41\mathrm{G}}$, and $\tau_{41\mathrm{v}}$ are the induction normal curvatures and the induction geodesic torsion, respectively, and their detailed derivation is provided in Reference[22].

Direction angle of the contact path at the reference point

Figure 6 shows the relative position of the pinion and gear when they are meshing at point M. Coordinate system $S_{0i}(O_i; \boldsymbol{i}_{0i}, \boldsymbol{j}_{0i}, \boldsymbol{k}_{0i})$ $(i = 1, 2)$ is rigidly connected to the machine frame. Origin O_i is the foot point of the common perpendicular of the axis of the pinion and the axis of the gear; axis $\boldsymbol{k}_{0i}$ coincides with the axis of the blank, and axis $\boldsymbol{j}_{0i}$ coincides with the common perpendicular. Origin O''_2 is in the center of the pitch circle of the gear at point M. Parameter E is the offset, and parameter Σ is the shaft angle.

By coordinate transformation, the gear tooth surface Σ_2 is represented in system S_{02} as (based on Fig. 6):

$$(\boldsymbol{r}_2)_{02} = A_{\mathrm{m2}}\boldsymbol{k}_{02} + \boldsymbol{M}_{202} \cdot (\boldsymbol{r}_2^*)_2, \tag{38}$$

Where

$$\boldsymbol{M}_{202} = \begin{bmatrix} cos(180^\circ - \varphi_{M2} + \varepsilon_2) & -sin(180^\circ - \varphi_{M2} + \varepsilon_2) & 0 & 0 \\ sin(180^\circ - \varphi_{M2} + \varepsilon_2) & cos(180^\circ - \varphi_{M2} + \varepsilon_2) & 0 & 0 \\ 0 & 0 & 1 & 0 \\ 0 & 0 & 0 & 1 \end{bmatrix}, \tag{39}$$

$$\varepsilon_2 = arcsin(sin\beta_{\mathrm{m12}} cos\delta_1 / sin\Sigma). \tag{40}$$

A_{m2} is the installment distance of the gear, β_{m12} is the difference between the spiral angles of the pinion and that of the gear, and δ_1 is the pitch angle of the pinion.

The vectors of the axes of coordinate system $S_{\mathrm{M}}(M, \boldsymbol{\alpha}_{2\mathrm{v}}, \boldsymbol{\alpha}_{2\mathrm{G}}, \boldsymbol{n}_2)$ are represented in system S_{02} as (based on Fig. 7):

$$(\boldsymbol{\alpha}_{2\mathrm{v}})_{02} = \boldsymbol{M}_{202} \cdot (\boldsymbol{\alpha}_{2\mathrm{v}})_2, \tag{41}$$

$$(\boldsymbol{\alpha}_{2\mathrm{G}})_{02} = \boldsymbol{M}_{202} \cdot (\boldsymbol{\alpha}_{2\mathrm{G}})_2, \tag{42}$$

$$(\boldsymbol{n}_2)_{02} = \boldsymbol{M}_{202} \cdot (\boldsymbol{n}_2^*)_2. \tag{43}$$

The angle velocity of the pinion is defined as $|\omega_1| = 1$ rad·s^{-1}, and the relative angular velocity is represented in system S_{02} by.

$$(\boldsymbol{\omega}_{12})_{02} = (\boldsymbol{\omega}_1)_{02} - (\boldsymbol{\omega}_2)_{02}, \tag{44}$$

$$(\boldsymbol{\omega}_1)_{02} = (\boldsymbol{k}_{01})_{02} = \boldsymbol{M}_{21} \cdot \boldsymbol{k}_{01}, \tag{45}$$

$$(\boldsymbol{\omega}_2)_{02} = -\frac{1}{i_{12}}(\boldsymbol{k}_{02})_{02}, \tag{46}$$

where i_{12} is the transmission ratio at point M, and.

$$\boldsymbol{M}_{21} = \begin{bmatrix} cos(-\Sigma) & 0 & sin(-\Sigma) & 0 \\ 0 & 1 & 0 & 0 \\ -sin(-\Sigma) & 0 & cos(-\Sigma) & 0 \\ 0 & 0 & 0 & 1 \end{bmatrix}. \tag{47}$$

The relative velocity of the pinion and gear at point M is represented by.

$$(\boldsymbol{v}_{12})_{02} = (\boldsymbol{\omega}_{12})_{02} \times (\boldsymbol{r}_2)_{02} + (\boldsymbol{\omega}_1)_{02} \times \left(E \cdot \boldsymbol{j}_{02}\right). \tag{48}$$

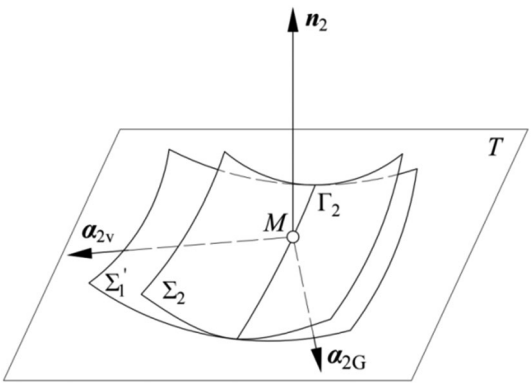

Figure 7. Relative positions of Σ_2 and Σ_1 and the coordinate system.

In the meshing process, surfaces Σ_1 and Σ_2 are in point contact continuously, and it can be assumed that imaginary tooth surfaces Σ_2' and Σ_1' is obtained from the envelopes of surfaces Σ_1 and Σ_2, and they are in line contact respectively. $\boldsymbol{\alpha}_{1v}$ and $\boldsymbol{\alpha}_{2v}$ are the vectors for the directions of the tooth trace of the pinion and the gear. At point M, $\boldsymbol{\alpha}_{1v} = \boldsymbol{\alpha}_{2v}$. Surfaces Σ_2 and Σ_1', as shown in Fig. 7, are in line contact. Γ_2 is the contact path. The relative positions of Σ_1 and $\Sigma_2'$are the same as those of Σ_2 and Σ_1'.

Tooth surface Σ_1 is in conjugation with surface Σ_2'; thus, the unit normal vector of the instantaneous contact line is obtained as.

$$(\boldsymbol{N}_{12})_{02} = N_{12v} \cdot (\boldsymbol{\alpha}_{2v})_{02} + N_{12G} \cdot (\boldsymbol{\alpha}_{2G})_{02}, \tag{49}$$

Here,

$$N_{12v} = \kappa_{1v}(\boldsymbol{v}_{12})_{02} \cdot (\boldsymbol{\alpha}_{2v})_{02} + \tau_{1v}(\boldsymbol{v}_{12})_{02} \cdot (\boldsymbol{\alpha}_{2G})_{02} + (\boldsymbol{\omega}_{12})_{02} \cdot (\boldsymbol{\alpha}_{2G})_{02}, \tag{50}$$

$$N_{12G} = \tau_{1v}(\boldsymbol{v}_{12})_{02} \cdot (\boldsymbol{\alpha}_{2v})_{02} + \kappa_{1v}(\boldsymbol{v}_{12})_{02} \cdot (\boldsymbol{\alpha}_{2G})_{02} - (\boldsymbol{\omega}_{12})_{02} \cdot (\boldsymbol{\alpha}_{2v})_{02}. \tag{51}$$

Tooth surface Σ_2 is in conjugation with tooth surface Σ_1'; thus, the unit normal vector of the instantaneous contact line is obtained as.

$$(\boldsymbol{N}_{21})_{02} = N_{21v}(\boldsymbol{\alpha}_{2v})_{02} + N_{21G}(\boldsymbol{\alpha}_{2G})_{02}, \tag{52}$$

Here,

$$N_{21v} = -\kappa_{2v}(\boldsymbol{v}_{12})_{02} \cdot (\boldsymbol{\alpha}_{2v})_{02} - \tau_{2v}(\boldsymbol{v}_{12})_{02} \cdot (\boldsymbol{\alpha}_{2G})_{02} - (\boldsymbol{\omega}_{12})_{02} \cdot (\boldsymbol{\alpha}_{2G})_{02}, \tag{53}$$

$$N_{21G} = -\tau_{2v}(\boldsymbol{v}_{12})_{02} \cdot (\boldsymbol{\alpha}_{2v})_{02} - \kappa_{2v}(\boldsymbol{v}_{12})_{02} \cdot (\boldsymbol{\alpha}_{2G})_{02} + (\boldsymbol{\omega}_{12})_{02} \cdot (\boldsymbol{\alpha}_{2v})_{02}. \tag{54}$$

The unit vectors tangent to the contact path at point M are denoted by $\boldsymbol{\alpha}_1$ and $\boldsymbol{\alpha}_2$ for the pinion and gear tooth surface, shown as Fig. 8, respectively. The direction angle of $\boldsymbol{\alpha}_i$ to $\boldsymbol{\alpha}_{2v}$ is defined as v_i ($i = 1, 2$):

$$\boldsymbol{\alpha}_i = cosv_i \cdot \boldsymbol{\alpha}_{2V} + sinv_i \cdot \boldsymbol{\alpha}_{2G}. \tag{55}$$

The area around reference point M meets the geometry condition of the tooth contact along the contact path: reference point M is the common point of both tooth surfaces, and a common normal line for both tooth surfaces exists at reference point M. Accordingly, angle v_i is obtained by the following equations:

$$tanv_2 = \frac{-(\kappa_{12V} + \tau_{12V})tan\theta_{12}}{\kappa_{12G}tan\theta_{12} + \tau_{12V}}, \tag{56}$$

$$tanv_1 = \frac{-(\kappa_{12V} + \tau_{12V})tan\theta_{21}}{\kappa_{12G}tan\theta_{21} + \tau_{12V}}, \tag{57}$$

Where

$$tan\theta_{12} = \frac{N_{12V}}{N_{12G}}, \tag{58}$$

$$tan\theta_{21} = \frac{N_{21V}}{N_{21G}}. \tag{59}$$

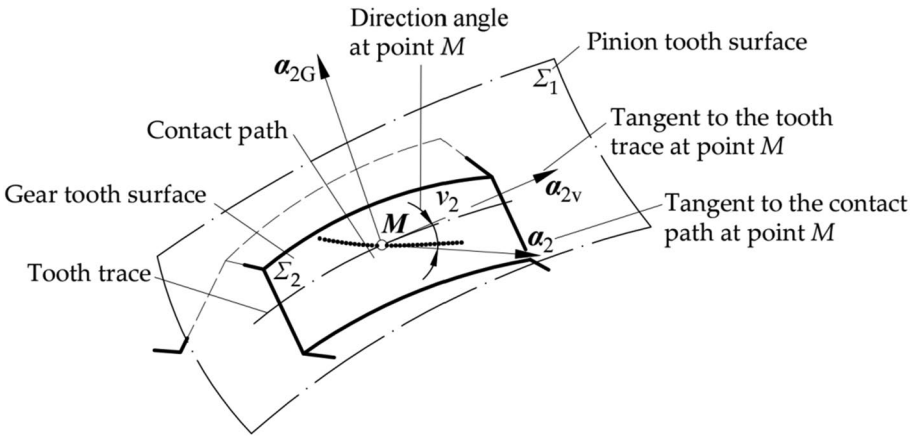

Figure 8. Position of the direction angle of the contact path.

Influence of the Angular Setting of the Head Cutter on the Direction of the Contact Path

In the Spirac system, the installment of the head cutter is determined by parameters E_{xi} and q_i for the gear if $i = 2$ and for the pinion if $i = 1$[22]. E_{xi} is corrected to satisfy the requirement of the spiral angle at the reference point, whereas q_i is not corrected. To further satisfy the requirement of the direction angle of the contact path, one more parameter is required. Thus, q_1 is chosen, and its influence on the contact path is investigated.

A numerical example is considered to analyze the influence, and Table 1 shows the main design parameters of the gear and the pinion.

Figure 9 shows the result of the contact path on the gear tooth surfaces obtained by correcting the value of q_1. The dotted lines with " + " signify the contact paths when $\Delta q_1 = +0.0003$ rad, the dotted lines with " − " signify the contact paths when $\Delta q_1 = -0.0003$ rad, and the solid lines signify the contact paths when the value is not corrected.

In Fig. 9, the positive correction of q_1 increases the angles between the contact path and the tooth trace on the concave and convex tooth surfaces simultaneously, whereas the negative correction decreases the angles. Meanwhile, the positive correction makes the contact paths on the concave and convex tooth surfaces move to the tooth heel simultaneously, whereas the negative correction has the reverse effect.

The result proves the validity of the angular setting of the head cutter q_1 to control the direction of the contact path. Considering its influence on the contact path, q_1 is added to control the symmetry of the contact paths on the concave and convex tooth surfaces of the gear.

Building equations

In the face hobbing method, the concave and convex tooth surfaces of the pinion or the gear are cut simultaneously under a single set of machine tool settings. Equations (1–60), described above, can be applied to evaluate the concave tooth surfaces of the pinion and the gear with the replacement of parameters u_{1i}, ψ_{1i}, and α_{1i}, and u_{2e}, ψ_{2e}, and α_{2e} with the original parameters (u_1, ψ_1, and α_1, and u_2, ψ_2, and α_2) and the convex tooth surfaces with the replacement of parameters u_{1e}, ψ_{1e}, and α_{1e}, and u_{2i}, ψ_{2i}, and α_{2i} with the original parameters (u_1, ψ_1, and α_1, and u_2, ψ_2, and α_2).

If the contact paths of the concave and convex tooth surfaces are symmetrical, parameters v_{1e} and v_{1i} will be related by the following equation:

$$v_{1e} = -v_{1i}. \tag{60}$$

Items			Pinion		Gear
Number of teeth	z	(–)	10		41
Shaft angle	Σ	(°)		90	
Mean normal module	m_n	(mm)		3.3342	
Offset	E	(mm)		20	
Face width	b	(mm)	33		30
Mean spiral angle	β_m	(°)	50.01LH		37.1344RH
Pressure angle	α_n	(°)		20	
Addendum coefficient	h^*	(–)		1	
Bottom clearance coefficient	c^*	(–)		0.25	
Addendum	h_a	(mm)	4.67		2
Whole depth height	h	(mm)		7.5	
Reference cone angle	δ	(°)	17.614		71.9607
Number of cutter tarts	z_0	(–)		11	
Cutter radius	r_0	(mm)		74	
Tilt angle	χ	(°)	5		4

Table 1. Design parameters for the numerical example.

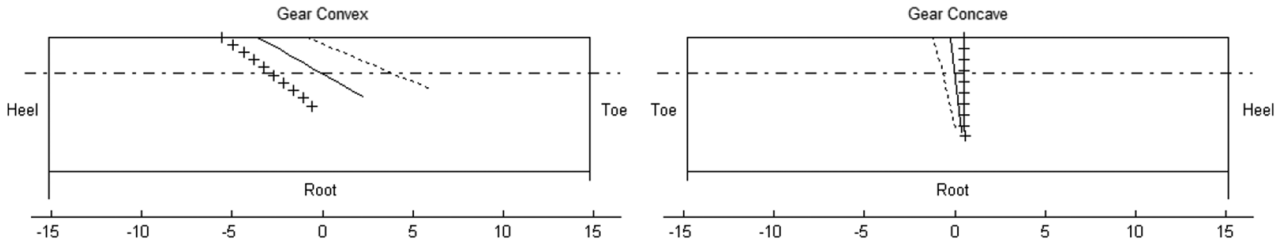

Figure 9. Influence of q4 on the contact path.

The current computation of machine tool settings for the Spirac hypoid gears is based on three conditions at the reference point: (a) the reference point is at the prescribed location, (b) the pressure angle at the reference point is equal to the theoretical value, and (c) the spiral angle at the reference point is equal to the theoretical value. The equations are.

$$\begin{cases} r^r_{mjk} = r_{m2} \\ r^n_{mjk} = 0 \\ \alpha_{mjk} = \alpha_{mk} \\ \beta_{mjk} = \beta_{m2} \end{cases} (j = 4,2; k = i, e), \tag{62}$$

Where r^r_{mjk} and r^n_{mjk} are the radial and axial positions of the reference point, respectively, on tooth surface Σ_j in coordinate system S_j; r_{m2} is the radius of the reference circle at point M; $\boldsymbol{\alpha}_{m4i}$ and $\boldsymbol{\alpha}_{m4e}$, and $\boldsymbol{\alpha}_{m2e}$ and $\boldsymbol{\alpha}_{m2i}$ are the normal pressure angles of the concave and convex tooth surfaces of the generating gear of pinion and the gear at the reference point, respectively; α_{mi} and α_{me} are the theoretical values of the normal pressure angles; β_{m4i} and β_{m4e}, and β_{m2e} and β_{m2i} are the spiral angles of the concave and convex tooth surfaces of the generating gear of pinion and the gear at the reference point, respectively; β_{m2} is the theoretical value of the spiral angle at the reference point.

Equation (61) consists of 16 nonlinear equations, which contain 16 unknowns, u_{1k}, ψ_{1k}, u_{2k}, ψ_{2k}, E_{x1}, E_{x2}, α_{1k}, α_{2k}, δ_{40}, and δ_{M2}, for solving for a set of values. To achieve symmetry of the contact paths, angle q_1 is taken as an unknown, and Eq. (60) is used for another function. Overall, 17 equations obtained from Eqs. (60) and (61) are applied to solve for the 17 unknowns to achieve the final values of the machine tool settings.

Analysis of the symmetry of the contact path

Table 1 lists the design parameters for the example hypoid gear pair. By the original method which is currently used for calculation[22], the values of the machine tool settings are obtained and listed in Tables 2, and 3 lists the results of the conditions. The output of the tooth contact analysis (TCA) is shown in Fig. 10a.

Items		Concave		Convex
1) Data of the gear				
Distance parameter of the blade	u_2(mm)	−1.4909		−1.3537
Angle parameter of the head cutter	ψ_2(°)	0.0198		−0.1392
Radial setting of the head cutter	E_{x2}(mm)		98.6396	
Blade angle	α_2(°)	−26.0412		13.8861
Angle of installment	δ_{M2}(°)		72.0903	
2) Data of the pinion				
Distance parameter of the blade	u_1(mm)	1.4705		1.3759
Angle parameter of the head cutter	ψ_1(°)	0.1771		−0.0454
Radial setting of the head cutter	E_{x1}(mm)		98.7660	
Blade angle	α_1(°)	−22.5719		17.3196
Pitch angle of the generating gear	δ_4(°)		68.8477	
Angular setting of the head cutter	q_1(°)		55.5783	

Table 2. Machine tool settings by the original method for the numerical example.

Items		Concave		Convex
1) Data of the gear				
Radial position of the reference point	r^r_{m2}(mm)	85.7373		85.7373
Axial positions of the reference point	r^n_{m2}(°)	0		0
Spiral angle at the reference point	β_{m2}(mm)	37.1344		37.1344
Pressure angle at the reference point	α_{n2}(°)	22.1180		17.8820
2) Data of the generating gear of the pinion				
Radial position of the reference point	r^r_{m4}(mm)	85.7373		85.7373
Axial positions of the reference point	r^n_{m4}(°)	0		0
Spiral angle at the reference point	β_{m4}(mm)	37.1344		37.1344
Pressure angle at the reference point	α_{n4}(°)	17.8820		22.1180
Direction angle of the contact paths	v_1(°)	16.0206		−38.1097

Table 3. Results obtained by the original method for the numerical example.

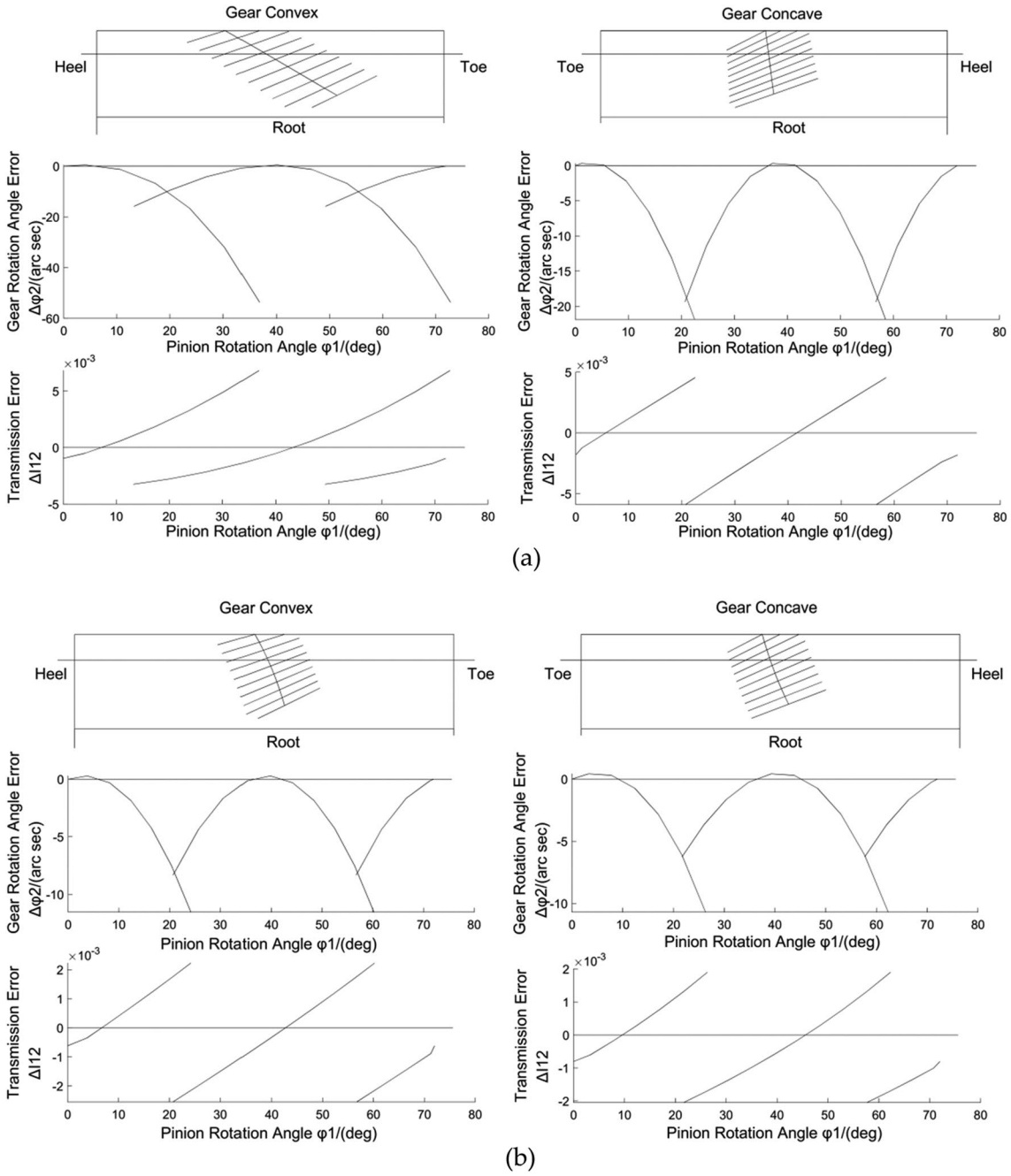

Figure 10. TCA outputs with the (**a**) original and (**b**) new methods.

By the new method proposed in this paper, the values of the machine tool settings are obtained and listed in Tables 4, and 5 lists the results obtained under the different conditions. The outputs of the TCA are shown in Fig. 10b.

Tables 2 and 4 show that the machine tool settings for the gear are modified and determined to be equal, whereas the machine tool settings for the pinion change. Tables 3 and 5 show that the values obtained by the two methods, related to the position of the reference point, the pressure angle, and the spiral angle, are both equal to the theoretical values. Table 3 shows that the direction angle of the contact paths on the concave tooth surface is not equal to the angle on the convex by the original method. In order to obtain a good meshing performance, they need to be modified artificially and repeatedly by correcting the machine tool settings. However, the direction angles of the contact paths on the concave and convex tooth surfaces of the gear obtained by the proposed method are equal in Table 5. This method is practicable and effective for impacting the meshing performance.

In Fig. 10a, there are significant differences in the tooth contact quality and the motion error between the concave and convex tooth surfaces: (i) both contact paths are not symmetrical; (ii) the convex tooth surface of the gear has a small rotation angle error but a long contact zone, which increases the gear sensitivity; and (iii) although the concave tooth surface has a good contact zone, it has a large rotation angle error.

Items		Concave		Convex
1) Data of the gear				
Distance parameter of the blade	u_2(mm)	− 1.4909		− 1.3537
Angle parameter of the head cutter	ψ_2(°)	0.0198		− 0.1392
Radial setting of the head cutter	E_{x2}(mm)		98.6396	
Blade angle	α_2(°)	− 26.0412		13.8861
Angle of installment	δ_{M2}(°)		72.0903	
2) Data of the pinion				
Distance parameter of the blade	u_1(mm)	0.9016		0.6749
Angle parameter of the head cutter	ψ_1(°)	− 9.4321		− 9.8387
Radial setting of the head cutter	E_{x1}(mm)		98.8282	
Blade angle	α_1(°)	− 26.5512		13.2689
Pitch angle of the generating gear	δ_4(°)		71.4439	
Angular setting of the head cutter	q_1(°)		65.2102	

Table 4. Machine tool settings obtained by the proposed method.

Items		Concave		Convex
1 Data of the gear				
Radial position of the reference point	r^r_{m2}(mm)	85.7373		85.7373
Axial positions of the reference point	r^n_{m2}(°)	0		0
Spiral angle at the reference point	β_{m2}(mm)	37.1344		37.1344
Pressure angle at the reference point	α_{n2}(°)	22.1180		17.8820
2 Data of the generating gear of the pinion				
Radial position of the reference point	r^r_{m4}(mm)	85.7373		85.7373
Axial positions of the reference point	r^n_{m4}(°)	0		0
Spiral angle at the reference point	β_{m4}(mm)	37.1344		37.1344
Pressure angle at the reference point	α_{n4}(°)	17.8820		22.1180
Direction angle of the contact paths	v_1(°)	31.8615		− 31.8615

Table5. Results obtained by the proposed method.

In Fig. 10b, the contact paths on the concave and convex tooth surfaces are approximately symmetrical, the motion errors are approximately equal, and the meshing characteristics are approximate. Thus, the proposed method for controlling the direction angle of the contact path at the reference point is effective, and it can improve the tooth contact quality and the transmission performance.

Conclusion

In this paper, a novel optimization method is presented for determining machine tool settings specific to Spirac hypoid gears, aiming to achieve optimal meshing performance with greater efficiency.

In the existing Spirac system, the pinion is cut by the generated method, the gear is cut by the non-generated method, which provides a higher production, but the meshing performance cannot be predicted and controlled. It needs to be modified artificially and repeatedly by correcting the machine tool settings during the tooth contact analysis. In the proposed method, the symmetry of the contact paths on the concave and convex tooth surfaces of the gear is controlled to achieve optimal meshing performance with greater efficiency. The direction angles of the two contact paths are equated to estimate their symmetry, achieved by modifying the angular setting of the head cutter when cutting the pinion. The results show that the contact paths on the concave and convex tooth surfaces are approximately symmetrical and the transmission errors of both sides are comparable.

Data availability

All data generated or analyzed during this study are included in this published article.

Received: 25 December 2023; Accepted: 17 May 2024
Published online: 21 May 2024

References

1. Stadtfeld, H. J. Hand book of bevel and hypoid gears: calculation, manufacturing, optimization, Rochester Institute of Technology, (1993).

2. Kolivand, M. & Kahraman, A. A load distribution model for hypoid gears using ease-off topography and shell theory. *Mech. Mach. Theor.* **44**, 1848–1865. https://doi.org/10.1016/j.mechmachtheory.2009.03.009 (2009).
3. Wang, X. L., Lu, J. W., Gu, X. G. & Yang, S. Q. A global synthesis approach for optimizing the meshing performance of hypoid gears based on a swarm intelligence algorithm. *Proc. Inst Mech. Eng. C* **235**, 1368–1388 (2021).
4. Zhou, Z., Tang, J. & Ding, H. Accurate modification methodology of universal machine tool settings for spiral bevel and hypoid gears. *Proc. Inst. Mech. Eng. B* **232**, 339–349. https://doi.org/10.1177/0954405416640173 (2018).
5. Litvin, F. L. Theory of gearing. NASA Reference Publication 1212, 1989.
6. Litvin, F. L., Zhang, Y. Local synthesis and tooth contact analysis of face-milled spiral bevel gears, NASA Contractor Report 4342, (1991).
7. Litvin, F. L., Fuentes, A. Gear geometry and applied theory (2nd ed), (Cambridge University Press, 2004).
8. Wang, P. Y. & Fong, Z. H. Fourth-order kinematic synthesis for face-milling spiral bevel gears with modified radial motion (MRM) correction. *J. Mech. Des.* **128**, 457–467. https://doi.org/10.1115/1.2168466 (2006).
9. Wu, X. C., Mao, S. M. & Wu, X. T. On function-oriented design of point-contact tooth surfaces. *Mech. Sci. Technol.* **19**, 347–349 (2000).
10. Dong, X. Z. Design and manufacture for epicycloidal spiral bevel and hypoid gears, (China Machine Press, 2002).
11. Fan, Q. Kinematical simulation of face hobbing indexing and tooth surface generation of spiral bevel and hypoid gears. *Gear Technol.* **23**, 30–38 (2006).
12. Fan, Q. Tooth surface error correction for face-hobbed hypoid gears. *J. Mech. Des.* https://doi.org/10.1115/1.4000646 (2010).
13. Artoni, A., Gabiccini, M. & Kolivand, M. Ease-off based compensation of tooth surface deviations for spiral bevel and hypoid gears: Only the pinion needs corrections. *Mech. Mach. Theor.* **61**, 84–101. https://doi.org/10.1016/j.mechmachtheory.2012.10.005 (2013).
14. Kolivand, M. & Kahraman, A. An ease-off based method for loaded tooth contact analysis of hypoid gears having local and global surface deviations. *J. Mech. Des.* https://doi.org/10.1115/1.4001722 (2010).
15. Li, G. & Zhu, W. D. An active ease-off topography modification approach for hypoid pinions based on a modified error sensitivity analysis method. *J. Mech. Des.* https://doi.org/10.1115/1.4043206 (2019).
16. Simon, V. Multi-objective optimization of hypoid gears to improve operating characteristics. *Mech. Mach. Theor.* **146**, 103727 (2019).
17. Artoni, A., Gabiccini, M., Guiggiani, M. & Kahraman, A. Multi-objective ease-off optimization of hypoid gears for their efficiency, noise, and durability performances. *J. Mech. Des.* https://doi.org/10.1115/1.4005234 (2011).
18. Shih, Y. P. & Fong, Z. H. Flank correction for spiral bevel and hypoid gears on a six-axis CNC hypoid generator. *J. Mech. Des.* https://doi.org/10.1115/1.2890112 (2008).
19. Shih, Y. P., Fong, Z. H. & Lin, G. C. Y. Mathematical model for a universal face hobbing hypoid gear generator. *J. Mech. Des.* **129**, 38–47. https://doi.org/10.1115/1.2359471 (2007).
20. Gonzalez-Perez, I. & Fuentes-Aznar, A. Conjugated action and methods for crowning in face-hobbed spiral bevel and hypoid gear drives through the Spirac system. *Mech. Mach. Theor.* **139**, 109–130. https://doi.org/10.1016/j.mechmachtheory.2019.04.011 (2019).
21. Du, J. F. & Fang, Z. D. An active tooth surface design methodology for face-hobbed hypoid gears based on measuring coordinates. *Mech. Mach. Theor.* **99**, 140–154. https://doi.org/10.1016/j.mechmachtheory.2016.01.002 (2016).
22. Dong, X. Z. Theoretical foundation of gear meshing. (China Machine Press, 1989).

Author contributions

Jiamin Xuan and Haitao Li wrote the main manuscript text and Wei Zhang prepared figures 1-6. The drawings in figures 7-10 were drawn by the author Jiamin Xuan. All authors reviewed the manuscript.

Funding

This work was support by the Key Research and Development Program of Zhejiang Province (No. 2022C01195, 2023C03158), Public Projects of Zhejiang Province (No. LGG21E060002), Key Science and Technology Project of Hangzhou (No. 2023SZD0041), General Scientific Research Program of Zhejiang Provincial Department of Education (No. Y201941541) and ZIME Science and Education Integration Cultivation and Incubation Engineering Project (No. A027120012).

Competing interests

The authors declare no competing interests.

Additional information

Correspondence and requests for materials should be addressed to J.X.